Optics Letters

Single camera shot interferenceless coded aperture correlation holography

Mani Ratnam Rai,†,* A. Vijayakumar,† and Joseph Rosen

Department of Electrical and Computer Engineering, Ben-Gurion University of the Negev, P.O. Box 653, Beer-Sheva 8410501, Israel
**Corresponding author: maniratnam1991@gmail.com*

Received 12 July 2017; revised 3 September 2017; accepted 5 September 2017; posted 7 September 2017 (Doc. ID 302253); published 29 September 2017

We propose a new scheme for recording an incoherent digital hologram by a single camera shot. The method is based on a motionless, interferenceless, coded aperture correlation holography for 3D imaging. Two random-like coded phase masks (CPMs) are synthesized using the Gerchberg–Saxton algorithm with two different initial random phase profiles. The two CPMs are displayed side by side and used as the system aperture. Light from a pinhole is introduced into the system, and two impulse responses are recorded corresponding to the two CPMs. The two impulse responses are subtracted, and the resulting intensity profile is used as a reconstructing hologram. A library of reconstructing holograms is created corresponding to all possible axial locations. Following the above training stage, an object is placed within the axial limits of the library, and the intensity patterns of a single shot, corresponding to the same two CPMs, are recorded under identical conditions to generate the object hologram. The image of the object at any plane is reconstructed by a cross-correlation between the object hologram and the corresponding reconstructing hologram from the library.

OCIS codes: (170.1630) Coded aperture imaging; (090.1995) Digital holography; (110.0110) Imaging systems; (110.0180) Microscopy; (050.0050) Diffraction and gratings; (110.2945) Illumination design.

https://doi.org/10.1364/OL.42.003992

Incoherent digital holography systems possess numerous advantages over their coherent counterparts because they do not require expensive and high power lasers, and therefore do not have to deal with problems such as edge ringing effects and speckle noise during imaging [1–3]. Besides, the spatial bandwidth of an incoherent imaging system is twice that of an equivalent coherent imaging system with an identical numerical aperture (NA) [4]. Moreover, incoherent holographic systems can image self-luminous objects as, for example, astronomical bodies and florescent specimens [5,6]. An incoherent digital holography system termed Fresnel incoherent correlation holography (FINCH) was developed based on the self-reference holography principle and demonstrated the possibility to achieve improved resolution in comparison with other imaging systems [7–9]. Another self-reference holography technique based on FINCH called coded aperture correlation holography (COACH) was developed recently to solve the axial resolution limitation of FINCH at the expense of lateral resolution. COACH exhibited the same lateral and axial resolution of regular imaging with the additional capability of 3D holographic imaging [10].

One of the disadvantages of COACH is the intrinsic background noise generated during reconstruction. Different noise reduction techniques such as hybridization and averaging techniques were developed to suppress the background noise at the expense of axial resolution and time resolution, respectively [11]. A modified version of COACH for 4D imaging in three spatial dimensions and wavelength with a diffractive objective lens and using the averaging technique has been demonstrated [12]. Recently, we have discovered that in COACH, with random-like coded phase masks (CPMs), the information of the 3D shape of an object is present not only in the phase of the diffracted wave but also in its amplitude. Therefore, two-wave interference that records the phase information is no longer necessary in the case of COACH to retrieve the information of the 3D image of the object. The intensity patterns of the light diffracted by the object and modulated by the CPMs are sufficient to reconstruct the object if the impulse response recorded under identical conditions is known. The principle of interferenceless COACH (I-COACH) has been recently demonstrated [13].

In this study, we present an advanced optical configuration of I-COACH in which the digital hologram of the object is recorded by a single camera shot. To be accurate, the operation of a single shot refers only to the post-training stage of the system. Recording a hologram by a single camera shot enables the acquisition of a holographic video of dynamic scenes in a regular video rate. In the past, several video digital holography techniques for recording and reconstructing dynamic 3D scenes have been developed [14–16]. However, the proposed technique has an optical configuration as simple as a regular imaging system, without two-wave interference and without using laser light.

In the previous I-COACH [13], the light diffracted from the object was modulated by a CPM (CPM1) synthesized using the Gerchberg–Saxton algorithm (GSA), and the corresponding

intensity pattern I_1 was recorded. Under identical conditions but with different CPMs (CPM2 and CPM3), second and third intensity patterns, namely I_2 and I_3, were recorded by second and third camera shots, respectively. The three intensity patterns were multiplied with three different phase values, namely $\theta_{1,2,3} = 0$, $2\pi/3$ and $4\pi/3$ and combined as $H_{\mathrm{PSH}} = I_1 \exp(j\theta_1) + I_2 \exp(j\theta_2) + I_3 \exp(j\theta_1)$, where H_{PSH} is called the point spread hologram (PSH). In the training stage of the system, a library of PSHs was created by shifting the location of the point object to all possible axial locations but with the same three CPMs and by repeating the above-mentioned process. After completing the training phase, an object was then placed within the axial boundaries of the PSH library, and the object hologram was obtained from the superposition of three intensity patterns taken by three camera shots and using the same three above mentioned CPMs. The image of the object at any z plane was reconstructed by correlating the object hologram with the corresponding PSH from the library. The GSA used in the case of I-COACH was constrained to yield a pure phase function in the sensor plane. However, because the image sensor was not located at the Fourier plane of the CPM, the Fourier relation between the CPM and the sensor plane was not satisfied in the experiment. This means that the Fourier-based GSA does not match the experimental setup, and hence the noise is not reduced as expected. Therefore, the averaging technique was still needed in order to reduce the background noise during reconstruction, in addition to the phase only filtering (POF) technique [9]. Thus, the time resolution of I-COACH was not minimal.

In the proposed single camera shot I-COACH (SCS-I-COACH), the condition of Fourier transform between the two GSA domains is accurately satisfied. A spherical positive lens is introduced at the CPM plane such that the sensor plane is located at the focal plane of the lens, which is also the Fourier plane for the CPM. In other words, the lens Fourier-transforms the CPM phase profiles onto its focal plane, whereas the quadratic phase multiplying the transform does not affect the intensity sensor. As a consequence, the GSA constraint to render a pure phase function at the Fourier sensor plane is satisfied accurately. Therefore, the background noise is lower in this case compared with the previous I-COACH [13], and the averaging technique with multiple camera shots can be avoided. Additional reduction of the camera shots can be achieved by use of two rather than three different CPMs. Therefore, in this study, instead of three different CPMs, only two different CPMs were used, and the corresponding intensity patterns are combined as $I_1 - I_2$. The goal of superposing intensity patterns is to eliminate the bias term, which introduces substantial background noise in the cross-correlation process of the reconstruction. Of course, subtracting two positive patterns with the same bias value is enough to get bias-free holograms. The time resolution is improved further by simultaneously installing the CPM1 and CPM2 within the system aperture. In the case of two CPMs positioned simultaneously, the field of view (FOV) of SCS-I-COACH is supposed to be lower than that of I-COACH because the aperture area has to be shared between the two CPMs, and two corresponding intensity patterns share the sensor area. Hence, additional constraints have to be introduced in the GSA to limit the area of the pure phase function on the sensor plane.

The integration of the two CPMs in the same aperture is shown in Fig. 1. The two CPMs, namely CPM1 and CPM2, are synthesized using the GSA from two different initial random phase matrices. To separate the intensity patterns on the sensor plane, two CPMs are multiplied by two linear phases along the horizontal axis [in principle, any other axis can be as good, but the horizontal axis is chosen because the spatial light modulator (SLM) is widest along this axis] with equal cycle length and opposite phase sign. The GSA constraint at the sensor plane is designed such that the two intensity patterns are constant only over a limited area, and there is no overlap between the two intensities. The CPMs and the respective linear phases are multiplied with a quadratic phase matrix that covers the complete aperture and is used as a diffractive positive lens. This lens guarantees a Fourier transform of the CPM on the sensor plane. The resultant phase function is

$$\exp(j\Phi_{\mathrm{SLM}}) = \left[\{\exp(j\Phi_{\mathrm{CPM1}})L(\bar{s})\}\mathrm{Rect}\left(\frac{x+a}{d}\right) + \{\exp(j\Phi_{\mathrm{CPM2}})L(-\bar{s})\}\mathrm{Rect}\left(\frac{x-a}{d}\right)\right] Q\left(-\frac{1}{z_h}\right), \tag{1}$$

where a and d are the CPMs' location and width with respect to the center of the SLM. For an SLM with a width of D, d is half and a is a quarter of D. $L(\bar{v}) = \exp\{j2\pi(\lambda)^{-1}(v_x x + v_y y)\}$ is the linear phase, $Q(b) = \exp\{j\pi b(\lambda)^{-1}(x^2 + y^2)\}$ is the quadratic phase, z_h is the distance between the SLM and the sensor plane, and $\bar{s}$ is the sinus of slanted angles of the two waves toward the two centers on the sensor plane. If the width of the sensor plane is U, the two centers are at $\pm U/4$ and hence $(s_x, s_y) = (U/(4z_h), 0)$. Φ_{CPM1} and Φ_{CPM2} are the phase profiles of the two CPMs.

The optical configuration of SCS-I-COACH is shown in Fig. 2. The light diffracted from the central point object is collected and collimated by a lens L_2. In the absence of the phase masks, CPM1 and CPM2, the wave is deflected in two directions due to the two linear phase masks. The two deflected waves are focused on the sensor plane by the diffractive positive lens. Hence, we can use a well-known law in Fourier optics [4] in which the Fourier transform of any mask transparency located anywhere between the source and the image points is obtained at the image plane of the source point. Moreover, the center of the Fourier transform is coincident with the image of the source point. The dimensions of the Fourier transform

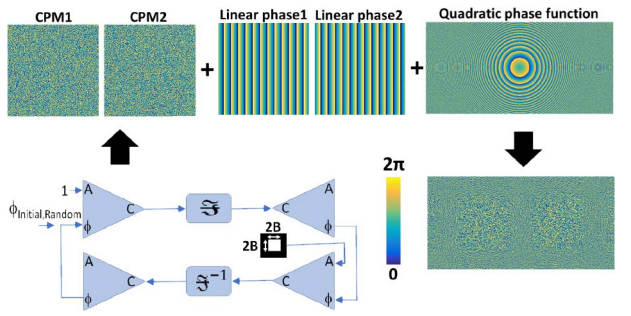

Fig. 1. Gerchberg–Saxton algorithm for generation of two CPMs and their integration with linear phases and a quadratic phase function for a single shot generation of the hologram.

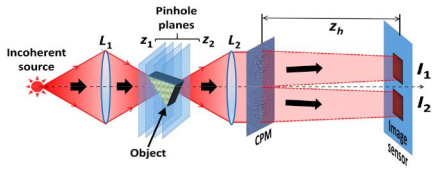

Fig. 2. Optical configuration of SCS-I-COACH.

function and the quadratic phase that multiplies it are dependent on the axial location of the mask. In the present setup, there are two image points to the single object point, and therefore, there are two Fourier transforms, one of CPM1 centered on $(U/4, 0)$ and the other of CPM2 centered on $(-U/4, 0)$. Thus, the intensity in the sensor plane is

$$I(u,v) = G_1(u - U/4, v) + G_2(u + U/4, v), \tag{2}$$

where $G_1 = |\Im\{\exp(j\Phi_{\mathrm{CPM1}})\}|^2$ and $G_2 = |\Im\{\exp(j\Phi_{\mathrm{CPM2}})\}|^2$. The two intensity patterns G_1 and G_2, corresponding to CPM1 and CPM2, respectively, are recorded, extracted, and subtracted one from the other. The resulting intensity pattern is termed PSH given by $H_{\mathrm{PSH}}(z_1) = G_1(u,v) - G_2(u,v)$. The point object is then shifted to different axial locations, and a library of PSH $\{H_{\mathrm{PSH}}(z_1)\ldots H_{\mathrm{PSH}}(z_2)\}$ is created.

An object is placed within the axial limits given by z_1 and z_2, but for simplicity, we analyze only the case of a planar object at the front focal plane of L_2 with the focal length of f_0. The object is a collection of incoherent source points distributed all over the profile of the object. Because the system from source to sensor is linear and space invariant for the intensity, the overall intensity response I_c on the sensor plane is the sum of the shifted impulse responses, as follows:

$$I_c = \sum_j G_1\left(u - \frac{z_h u_j}{f_0} - \frac{U}{4}, v - \frac{z_h v_j}{f_0}\right) + \sum_j G_2\left(u - \frac{z_h u_j}{f_0} + \frac{U}{4}, v - \frac{z_h v_j}{f_0}\right). \tag{3}$$

Each intensity pattern corresponding to each CPM and centered on $\pm U/4$ is extracted, and they are subtracted from each other. The resulting object hologram H_{obj} is

$$H_{\mathrm{obj}} = \sum_j G_1\left(u - \frac{z_h u_j}{f_0}, v - \frac{z_h v_j}{f_0}\right) - \sum_j G_2\left(u - \frac{z_h u_j}{f_0}, v - \frac{z_h v_j}{f_0}\right). \tag{4}$$

The image of the object is reconstructed by a cross-correlation between the object hologram and the PSH(f_0), as the following:

$$\begin{aligned} I_{\mathrm{img}} &= |H_{\mathrm{obj}} \otimes H_{\mathrm{PSH}}| \\ &= \left|\left[\sum_j G_1\left(u - \frac{z_h u_j}{f_0}, v - \frac{z_h v_j}{f_0}\right) - \sum_j G_2\left(u - \frac{z_h u_j}{f_0}, v - \frac{z_h v_j}{f_0}\right)\right] \otimes [G_1(u,v) - G_2(u,v)]\right| = \sum_j \Lambda\left(u_o - \frac{z_h u_j}{f_0}, v_o - \frac{z_h v_j}{f_0}\right) \\ &= O\left(\frac{f_0 u_o}{z_h}, \frac{f_0 v_o}{z_h}\right) = O\left(\frac{u_o}{M_T}, \frac{v_o}{M_T}\right), \end{aligned} \tag{5}$$

where $\otimes$ represents a two-dimensional correlation, Λ is a δ-like function, approximately equal to 1 around (0,0) and to small negligible values elsewhere, and $M_T = z_h/f_0$ is the lateral magnification of the imaging. Note that Λ is a δ-like function because both H_{obj} and H_{PSH} are bipolar with values over the entire real axis. Otherwise, if they are positive functions, the cross-correlation between them yields unaccepted background noise.

The experimental verification of SCS-I-COACH was carried out using a digital holography setup as shown in Fig. 3. The experimental setup consists of two illumination channels with identical LEDs emitting light at a wavelength of 635 nm (Thorlabs LED635L, 170 mW, $\lambda = 635$ nm, $\Delta\lambda = 10$ nm). Two identical lenses, L_{1A} and L_{1B}, were used to critically illuminate two objects: element 12.70 lp/mm (Thorlabs) of group 3 of the United States Air Force (USAF) resolution chart and 16 lp/mm (Edmund Optics) of the National Bureau of Standards (NBS). The distance from the lens L_{1A} and L_{1B} from their respective objects was 5 cm, while the diameter of the beam at the output of the lenses was 1.8 cm. The distance between the objects and the lens L_2, with a diameter of 2.5 cm and a focal length of $f_0 = 20$ cm, is about 20 cm. The distance between the lens L_2 and the phase-only reflective SLM (Holoeye PLUTO, 1920 × 1080 pixels, 8 μm pixel pitch, phase-only modulation) is 9.5 cm. The distance between the lens L_2 and the center of beam splitter BS_2 is 6 cm. The distance between the SLM and the image sensor (Hamamatsu ORCA-Flash4.0 V2 Digital CMOS, 2048 × 2048 pixels, 6.5 μm pixel pitch, monochrome) is $z_h = 25.4$ cm.

The GSA is designed to generate a pure phase function in the sensor plane. An additional constraint is added to limit the area of the pure phase function so that both intensity patterns corresponding to the two CPMs are captured within the area of the image sensor. In this case, an area of the pure phase function was selected to be 300 × 300 pixels out of 1000 × 1000. In the experimental setup, it is converted to 4.3 × 4.3 mm. The linear phase was chosen to be ±0.7°. Therefore, for a distance of $z_h = 25.4$ cm, the intensity patterns are shifted by a distance of approximately 3 mm from the optical axis.

In the training stage of the system, a pinhole with a diameter of 25 μm is mounted in channel 1, and channel 2 is blocked. The phase mask containing the two CPMs with the linear phases and the quadratic phase mask is displayed on the SLM. The light diffracted by the pinhole passes through a polarizer that is oriented along the active axis of the SLM to enable full modulation of light. The light modulated by the SLM is incident on the image sensor. The two intensity patterns captured by the image sensor are shown in Fig. 4(a). The two intensity patterns are extracted, and then one is subtracted from the other. The resulting bipolar pattern of PSH(f_0) is shown in Fig. 4(b). The location of the pinhole is shifted in steps of 1 mm, and a library of PSHs {PSH$(z_1 = 0)\ldots$PSH$(z_2 = 10$ mm$)$} is created.

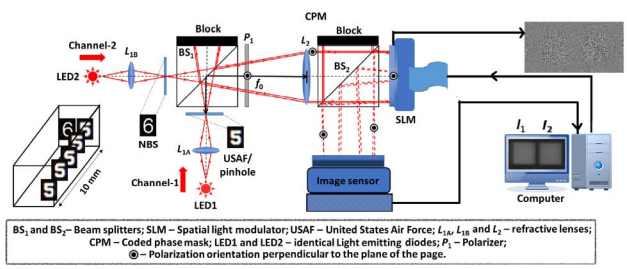

Fig. 3. Experimental setup of SCS-I-COACH with two illumination channels.

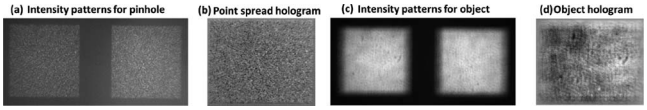

Fig. 4. Intensity patterns at the image sensor of (a) pinhole and (c) object in the system input. Hologram of (b) pinhole and (d) object.

Following the training stage, both optical channels are used simultaneously in acquiring the object hologram. The location of the NBS object is kept constant while the location of the USAF object is shifted in steps of 1 mm, and two-plane objects with different thicknesses are created. The two intensity patterns recorded by the image sensor for the two objects located at the focal plane of the lens L_2 are shown in Fig. 4(c). The two intensity patterns are extracted and subtracted from each other as before to obtain the object hologram shown in Fig. 4(d). The object hologram is then correlated with the POF version of the PSH(z) to reconstruct the image of the object at z. The object holograms, taken with various object positions, were reconstructed using the PSH library to obtain the reconstruction of the different planes of the object.

The reconstruction results are shown in Fig. 5. The different rows (11 rows) correspond to the different gaps between the two planar objects with a maximum gap of 10 mm. The columns correspond to the different PSHs used in the reconstruction process of Fig. 5. It can be noted that the background noise level is suppressed better than the earlier cases because of the use of the diffractive lens and Fourier relation, rather than Fresnel [10–13] relations between the CPM and the camera plane. GSA was found to yield better noise reduction when the pure phase function in the sensor plane is constrained to a larger area. But in order to share the area of the image sensor between the two intensity patterns, the area constraint is necessary in the sensor plane. For this reason, the FOV of SCS-I-COACH becomes limited. Therefore, in the case of SCS-I-COACH, the single shot ability is achieved at the expense of narrower FOV and also lower SNR. However, the single shot capability allows recording and reconstructing 3D videos in the standard rate. A dynamic hologram is recorded when the USAF chart is moved between the limits of the PSH library. The dynamic hologram is reconstructed using PSHs corresponding to different axial planes. The variation of the reconstruction along the diagonal direction from the figure at (Row 1, Column 1) to figure at (Row 6, Column 6) and then to figure at (Row 11, Column 1) is shown in Visualization 1. The reconstruction video perspective to different axial planes corresponding to the first 9 rows of Fig. 5 is shown in Visualization 2 simultaneously, a unique characteristic of holography video. This demonstrates the 4D imaging capability of SCS-I-COACH along the three spatial dimensions and time.

In conclusion, we have developed a motionless, interferenceless, incoherent digital holography technique that uses only single camera shot to acquire the object hologram of a 3D scene. SCS-I-COACH does not require more than a single phase mask, both in the training stage and in the object hologram acquisition. Therefore, the CPMs' profile along with the lens function and the linear phases can be integrated into a single phase mask fabricated using lithography techniques [17]. Finally, it should be noted that SCS-I-COACH is different

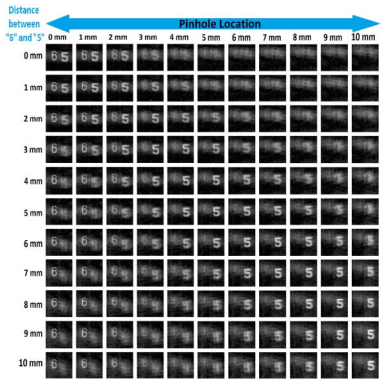

Fig. 5. Reconstruction results of the two-plane object made of "5" and "6" using PSHs corresponding to different axial locations. Each row is a different object hologram, whereas each column is a reconstruction in a different axial position. The 3D videos along different axial planes are shown in Visualization 1, Visualization 2, and Visualization 3.

from both confocal and deconvolution methods. In SCS-I-COACH, a single image of the scene is acquired without any further scanning, whereas in confocal imaging, the depth information is obtained by scanning either along the spatial axes or along the spectral axis. Deconvolution operates on images captured by a microscope with an aperture of a clear disc. In SCS-I-COACH, images are acquired by a system with an engineered aperture, designed in advance to enable efficient image sectioning.

Funding. Israel Science Foundation (ISF) (1669/16, 439/12).

[†]These authors contributed equally for this work.

REFERENCES

1. B. M. Oliver, Proc. IEEE **51**, 220 (1963).
2. P. S. Considine, J. Opt. Soc. Am. **56**, 1001 (1966).
3. J. P. Mills and B. J. Thompson, J. Opt. Soc. Am. A **3**, 704 (1986).
4. J. W. Goodman, *Introduction to Fourier Optics* (McGraw-Hill, 1968), Chap. 6, pp. 154–156 and Chap. 5.
5. E. Ribak, C. Roddier, F. Roddier, and J. B. Breckinridge, Appl. Opt. **27**, 1183 (1988).
6. B. W. Schilling, T.-C. Poon, G. Indebetouw, B. Storrie, K. Shinoda, Y. Suzuki, and M. H. Wu, Opt. Lett. **22**, 1506 (1997).
7. J. Rosen and G. Brooker, Opt. Lett. **32**, 912 (2007).
8. J. Rosen and G. Brooker, Nat. Photonics **2**, 190 (2008).
9. J. Rosen, N. Siegel, and G. Brooker, Opt. Express **19**, 26249 (2011).
10. A. Vijayakumar, Y. Kashter, R. Kelner, and J. Rosen, Opt. Express **24**, 12430 (2016).
11. A. Vijayakumar, Y. Kashter, R. Kelner, and J. Rosen, Appl. Opt. **56**, F67 (2017).
12. A. Vijayakumar and J. Rosen, Opt. Lett. **42**, 947 (2017).
13. A. Vijayakumar and J. Rosen, Opt. Express **25**, 13883 (2017).
14. O. Matoba, T. J. Naughton, Y. Frauel, N. Bertaux, and B. Javidi, Appl. Opt. **41**, 6187 (2002).
15. B. Javidi, I. Moon, S. Yeom, and E. Carapezza, Opt. Express **13**, 4492 (2005).
16. S. Zwick, T. Haist, M. Warber, and W. Osten, Appl. Opt. **49**, F47 (2010).
17. A. Vijayakumar and S. Bhattacharya, *Design and Fabrication of Diffractive Optical Elements with MATLAB* (SPIE, 2017), Chap. 8.